**Initiation of polarization.** Two factors appeared to be necessary to initiate the observed polarization of the cytoskeleton: HTLV-I infection of the cell and contact with another cell. It is not yet clear which molecules mediate these signals. HTLV-I Env protein is again a candidate for this function, because it is the only HTLV-I protein that is expressed intact on the outside of the infected cell. However, HTLV-I also up-regulates expression of certain adhesion molecules such as integrins (*19*, *20*), which will increase the likelihood of cell-cell adhesion. Furthermore, Yamamoto *et al*. (*20*) found that ligation of ICAM-1 on the cell surface induces expression of HTLV-I genes, which suggests the existence of a positive feedback loop between cell-cell adhesion and HTLV-I gene expression (fig. S3).

HTLV-I Gag protein, in complex with the HTLV-I genome, appears to be transported to the MTOC by a microtubule-dependent process. Microtubules have been shown to be involved in the intracellular transport of other viruses, e.g., adenovirus and herpesvirus (*21*–*23*).

The junction formed between an HTLV-I–infected T cell and another T cell shared two similarities—ordered talin domains and MTOC polarization—with the "immunological synapse" (*24*). However, in the present study the MTOC polarization occurred within the HTLV-I–infected cell, not toward the infected cell. Therefore, MTOC polarization was not triggered by recognition of HTLV-I antigens presented by a neighboring T cell, and the structures we report here cannot be considered an "immunological" synapse. The term "virological synapse" may be more appropriate.

HTLV-I can infect almost any mammalian cell in vitro, but in vivo it is almost confined to T cells, for unknown reasons (*25*–*27*). It is possible that T cell–specific factors are required either for efficient HTLV-I replication or for the process of cell-to-cell transfer reported here.

We conclude that HTLV-I exploits the normal physiology of the T cell to enable efficient cell-to-cell transmission by forming a close contact with the recipient cell and using the cytoskeleton to propel viral material into the recipient cell (fig. S3). Although HTLV-I has a peculiarly strong dependence on cell contact for efficient transmission of the virus between cells, it is possible that other lymphotropic viruses, such as HIV-1 (*28*, *29*), use a similar mechanism to spread between lymphocytes.

### References and Notes


1. T. Uchiyama, J. Yodoi, K. Sagawa, K. Takatsuki, H. Uchino, *Blood* **50**, 481 (1977).
2. A. Gessain *et al.*, *Lancet* **2**, 407 (1985).
3. M. Osame *et al.*, *Lancet* **1**, 1031 (1986).
4. N. E. Mueller, W. A. Blattner, in *Viral Infections of Humans: Epidemiology and Control*, A. S. Evans, R. Kaslow, Eds. (Plenum Medical Press, New York, 1997), pp. 785–813.
5. K. Okochi, H. Sato, Y. Hinuma, *Vox Sang* **46**, 245 (1984).
6. N. Yamamoto, M. Okada, Y. Koyanagi, M. Kannagi, Y. Hinuma, *Science* **217**, 737 (1982).
7. M. Popovic *et al.*, *Science* **219**, 856 (1983).
8. N. Fan *et al.*, *J. Clin. Microbiol.* **30**, 905 (1992).
9. D. Derse, S. A. Hill, P. A. Lloyd, H. Chung, B. A. Morse, *J. Virol.* **75**, 8461 (2001).
10. L. Delamarre, A. R. Rosenberg, C. Pique, D. Pham, M. C. Dokhelar, *J. Virol.* **71**, 259 (1997).
11. K. Nagy, P. Clapham, R. Cheingsong-Popov, R. A. Weiss, *Int. J. Cancer* **32**, 321 (1983).
12. S. R. Jassal, M. D. Lairmore, A. J. Leigh-Brown, D. W. Brighty, *Virus Res.* **78**, 17 (2001).
13. M. A. Sommerfelt *et al.*, *Science* **242**, 1557 (1988).
14. S. R. Jassal, R. G. Pohler, D. W. Brighty, *J. Virol.* **75**, 8317 (2001).
15. J. E. Hildreth, A. Subramanium, R. A. Hampton, *J. Virol.* **71**, 1173 (1997).
16. S. Daenke, S. A. McCracken, S. Booth, *J. Gen. Virol.* **80**, 1429 (1999).
17. I. Le Blanc *et al.*, *J. Virol.* **76**, 905 (2002).
18. C. Meric, P. F. Spahr, *J. Virol.* **60**, 450 (1986).
19. H. Valentin *et al.*, *J. Virol.* **71**, 8522 (1997).
20. A. Yamamoto, H. Hara, T. Kobayashi, *J. Neurol. Sci.* **151**, 121 (1997).
21. B. R. Cullen, *Cell* **105**, 697 (2001).
22. M. Suomalainen, M. Y. Nakano, K. Boucke, S. Keller, U. F. Greber, *EMBO J.* **20**, 1310 (2001).
23. H. Mabit *et al.*, *J. Virol.* **76**, 9962 (2002).
24. A. Grakoui *et al.*, *Science* **285**, 221 (1999).
25. K. Nagy, R. A. Weiss, P. R. Clapham, R. Cheinsong-Popov, in *Human T-Cell Leukemia/Lymphoma Viruses*, R. C. Gallo, Ed. (Cold Spring Harbor Laboratory Press, Cold Spring Harbor, NY, 1984), pp. 121–131.
26. J. H. Richardson, A. J. Edwards, J. K. Cruickshank, P. Rudge, A. G. Dalgleish, *J. Virol.* **64**, 5682 (1990).
27. E. Hanon *et al.*, *Immunity* **13**, 657 (2000).
28. D. S. Dimitrov *et al.*, *J. Virol.* **67**, 2182 (1993).
29. R. Pearce-Pratt, D. Malamud, D. M. Phillips, *J. Virol.* **68**, 2898 (1994).


30. We thank the staff and patients of St. Mary's Hospital for their cooperation, Q. Sattentau and D. M. Davis (Imperial College, UK) for helpful discussions, A. Barnard for help with the MTOC orientation experiments, and N. White (Sir William Dunn School of Pathology, University of Oxford, UK) for help with the use of the confocal microscope facility. This work was supported by The Wellcome Trust (UK).


**Supporting Online Material**

www.sciencemag.org/cgi/content/full/1080115/DC1
Materials and Methods
Figs. S1 to S3
Table S1
References


4 November 2002; accepted 28 January 2003
Published online 13 February 2003;
10.1126/science.1080115
Include this information when citing this paper.


# REPORTS

## Grain Boundary Scars and Spherical Crystallography


**A. R. Bausch,[1]* M. J. Bowick,[2]* A. Cacciuto,[3] A. D. Dinsmore,[4] M. F. Hsu,[5] D. R. Nelson,[5] M. G. Nikolaides,[1,5] A. Travesset,[6] D. A. Weitz[5]**



We describe experimental investigations of the structure of two-dimensional spherical crystals. The crystals, formed by beads self-assembled on water droplets in oil, serve as model systems for exploring very general theories about the minimum-energy configurations of particles with arbitrary repulsive interactions on curved surfaces. Above a critical system size we find that crystals develop distinctive high-angle grain boundaries, or scars, not found in planar crystals. The number of excess defects in a scar is shown to grow linearly with the dimensionless system size. The observed slope is expected to be universal, independent of the microscopic potential.


Spherical particles on a flat surface pack most efficiently in a simple lattice of triangles, similar to the arrangement of billiard balls at the start of a game. Such six-fold coordinated triangular lattices (*1*) cannot, however, be wrapped on the curved surface of a sphere; instead, there must be extra defects in coordination number. Soccer balls and $C_{60}$ fullerenes (*2*, *3*) provide familiar realizations of this fact; they have 12 pentagonal panels and 20 hexagonal panels. The necessary packing defects can be characterized by their topological or disclination charge, $q$, which is the departure of their coordination number $c$ from the preferred flat space value of 6 ($q = 6 - c$); a classic theorem of Euler (*4*, *5*) shows that the total disclination charge of any triangulation of the sphere must be 12 (*6*). A total disclination charge of 12 can be achieved in many ways, however, which makes the determination of the minimum-energy configuration of repulsive particles, essential for crystallography on a sphere, an extremely difficult problem. This difficulty was recognized nearly 100 years ago by J. J. Thomson (*7*), who attempted, unsuccessfully, to explain the periodic table in terms of rigid electron shells. Similar problems recur in fields as diverse as multielectron bubbles in superfluid helium (*8*), virus morphology (*9*–*11*), protein s-layers (*12*, *13*), and coding theory (*14*, *15*). Indeed, both the classic

Thomson problem, which deals with particles interacting through the Coulomb potential, and its generalization to other interaction potentials remain largely unsolved after almost 100 years (*16*–*18*).

The spatial curvature encountered in curved geometries adds a fundamentally new ingredient to crystallography, not found in the study of order in spatially flat systems. To date, however, studies of the Thomson problem and related problems have been limited to theory and computer simulation. As the number of particles on the sphere grows, isolated charge 1 defects are predicted to induce too much strain; this excess strain can be relieved by introducing additional dislocations, consisting of pairs of tightly bound 5-7 defects (*19*), which still satisfy Euler's theorem because their net disclination charge is zero. Dislocations, which are pointlike topological defects in two dimensions, disrupt the translational order of the crystalline phase but are less disruptive of orientational order (*19*). Although they play an essential role in crystallography on a spherical surface, the configuration and orientation of these excess defects remain undetermined and can only be fully understood through a combination of theory and experiment. Experimental realizations that probe the subtle structures have, however, been sorely lacking.

We present an experimental realization of the generalized Thomson problem that allows us to explore the lowest energy configuration of the dense packing of repulsive particles on a spherical surface. We create two-dimensional packings of colloidal particles on the surface of spherical water droplets and view the structures with optical microscopy. Above a critical system size, the thermally equilibrated colloidal crystals display distinctive high-angle grain boundaries, which we label "scars." These grain boundaries are found to end within the crystal, which is not observed to occur on flat surfaces because the energy penalty is too high.

Our experimental system is based on the self-assembly of 1-μm-diameter cross-linked polystyrene beads adsorbed on the surface of spherical water droplets (of radius $R$), themselves suspended in a density-matched toluene-chlorobenzene mixture (*20*). The particles are imaged with phase contrast, using an inverted microscope. The curvature of the spherical water droplet limits the imaged surface area to between 5 and 20% of the full surface area of the sphere, depending on the size of the droplet. After the center of mass of each bead has been determined, the lattice geometry is analyzed by Delaunay triangulation algorithms (*21*) appropriate to spherical surfaces.

We analyze the lattice configurations of a collection of 40 droplets. A typical small spherical droplet with system size $R/a = 4.2$, where $a$ is the mean particle spacing, is shown in Fig. 1A. The associated Delaunay triangulation is shown in Fig. 1B. The only defect is one isolated charge +1 disclination. Extrapolation to the entire surface of the sphere is statistically consistent with the required 12 total disclinations.

Qualitatively different results are observed for larger droplet sizes as defect configurations with excess dislocations appear. Although some of these excess dislocations are isolated, most occur in the form of distinctive (5−7−5−7−. . .−5) chains, each of net charge +1 (Fig. 1D). These chains form high-angle (30°) grain boundaries, or scars, which terminate freely within the crystal. Such a feature is energetically prohibitive in equilibrium crystals in flat space. Thus, although grain boundaries are a common feature of two-dimensional (2D) and 3D crystalline materials, arising from a mismatch of crystallographic orientations across a boundary, they usually terminate at the boundary of the sample in flat space because of the excessive strain energy associated with isolated terminal disclinations. Termination within the crystal is a feature unique to curved space. Thus, our results provide important guidance to determine the configuration of excess defects on a sphere.

To ascertain that the colloidal particles are equilibrated, we use particle-tracking routines and subsequent automated triangulation to measure the mobility of the observed screening dislocations. The diffusion of thermally excited colloid particles on the surface of the water droplets results in local rearrangements of the crystal structure. Thermal fluctuations create and destroy dislocations once every few seconds, on average, indicating that the defect arrays reach equilibrium much faster than the observation time of 10 to 60 min. The equilibration time can also be estimated by the time required for a dislocation to diffuse across typical defect structures. The measured diffusion constant allows us to calculate equilibration times that range from a few seconds to hundreds of seconds, depending on the size of the crystal. Because the spherical crystals exist for 10 to 60 min, the system has sufficient time to reach equilibrium. Thus, our observations reflect the equilibrium ground state, as opposed to

[1]Department of Physics, E22, Technische Universität München, 85747 München, Germany. [2]Physics Department, Syracuse University, Syracuse, NY 13244–1130, USA. [3]Fundamenteel Onderzoek der Materie Institute for Atomic and Molecular Physics, Kruislaan 407, 1098 SJ, Amsterdam, The Netherlands. [4]Department of Physics, University of Massachusetts, Amherst, MA 01003–4525, USA. [5]Department of Physics and Division of Engineering and Applied Sciences, Harvard University, Cambridge, MA 02138, USA. [6]Physics and Astronomy Department, Iowa State University, and Ames National Laboratory, Ames, IA 50011, USA.

*To whom correspondence should be addressed. E-mail: abausch@ph.tum.de (A.R.B.), bowick@physics.syr.edu (M.J.B.)

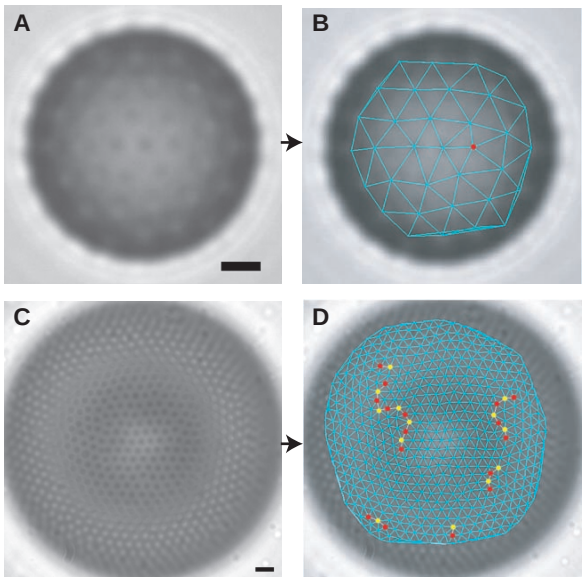


**Fig. 1.** Light microscope images of particle-coated droplets. Two droplets (**A**) and (**C**) are shown, together with their associated defect structures (**B**) and (**D**). (A) An ~13% portion of a small spherical droplet with radius $R$ = 12.0 μm and mean particle spacing $a$ = 2.9 μm ($R/a$ = 4.2), along with the associated triangulation (B). Charge +1(−1) disclinations are shown in red and yellow, respectively. Only one +1 disclination is seen. (C) A cap of spherical colloidal crystal on a water droplet of radius $R$ = 43.9 μm with mean particle spacing $a$ = 3.1 μm ($R/a$ = 14.3), along with the associated triangulation (D). In this case the imaged crystal covers ~17% of the surface area of the sphere. Bars [(A) and (C)], 5 μm.

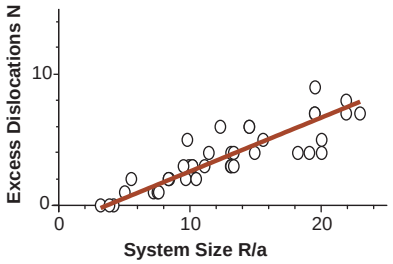


**Fig. 2.** Excess dislocations as a function of system size. The number of excess dislocations per minimal disclination $N$ as a function of system size $R/a$, with the linear prediction given by theory shown as a solid red line.

a history-dependent nonequilibrium effect, which is the case for crystals in flat space.

To quantify the behavior of the scars, we determine the number of excess dislocations per chain for each droplet, with the convention that dislocations are counted as part of the same array if they are within three lattice spacings, and plot the results as a function of $R/a$ (Fig. 2). Scars only appear for droplets with $R/a \geq 5$. These results provide a critical confirmation of a theoretical prediction that $R/a$ must exceed a threshold value $(R/a)_c \approx 5$, corresponding to $M \approx 360$ particles, for excess defects to proliferate in the ground state of a spherical crystal (*22*). The precise value of $(R/a)_c$ depends on details of the microscopic potential, but its origin is easily understood by considering just one of the 12 charge +1 disclinations required by the topology of the sphere. In flat space such a topological defect has an associated energy that grows quadratically with the size of the system, because it is created by excising a 60° wedge of material and gluing the boundaries together (*23*). The elastic strain energy associated with this defect grows as a function of the area. In the case of the sphere, the radius plays the role of the system size. As the radius increases, isolated disclinations become much more energetically costly. This elastic strain energy may be reduced by the formation of linear dislocation arrays, i.e., grain boundaries. The energy needed to create these additional dislocation arrays is proportional to a dislocation core energy $E_c$ and scales linearly with the system size. Such screening is inevitable in flat space (the plane) if one forces an extra disclination into the defect-free ground state. Unlike the situation in flat space, grain boundaries on the sphere can freely terminate (*22–26*), and our experimental results confirm these theoretical expectations.

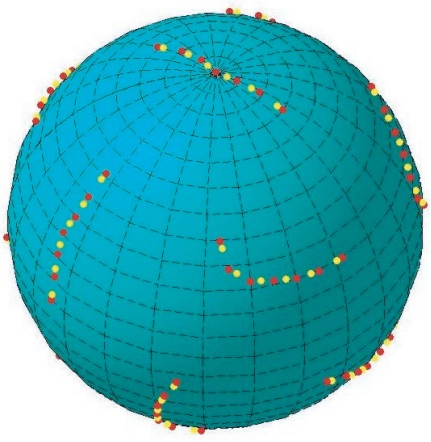

**Fig. 3.** Model grain boundaries. This image is obtained from a numerical minimization, based on the theory of (*22*), for a system size comparable to that of the droplet in Fig. 1, C and D.

One systematic approach to determining the ground state of a collection of $M$ particles distributed on the sphere and interacting through an arbitrary repulsive potential (*22*, *27*) treats the disclination defects themselves as the fundamental degrees of freedom, with the 6-coordinated particles forming a continuum elastic background. The agreement between the predicted and observed values of $(R/a)_c$ supports the validity of this theoretical approach. The original particle pair potential is replaced by a long-range defect pair potential given by

$$\chi(\beta) \propto R^2(1+\int_0^{[(1-\cos\beta)/2]} dz[\ln z/(1-z)])$$

for a pair of defects separated by an angular distance $\beta$. The potential is attractive for opposite-charged defects and repulsive for like-charged defects. The underlying microscopic potential enters only in determining the proportionality constant (equivalent to an elastic Young modulus) and $E_c$. Many predictions of this model are therefore universal in the sense that they are insensitive to the exact microscopic potential. This enables us to make definite predictions even though the colloidal potential is not precisely known. It also means that our model system serves as a prototype for any analogous system with repulsive interactions and spherical geometry. To further test the validity of this approach, we show a typical ground state for large $M$ in Fig. 3. The system size here is $R/a = 12$, similar to the droplet in Fig. 1D. The results are markedly similar to the experimentally observed configuration in Fig. 1D; the only difference is a result of thermal fluctuations, which break the two defect scars in the experiment. This agreement between theory and experiment also provides convincing evidence that these scars are essential components of the equilibrium crystal structure on a sphere.

The theory predicts that an isolated charge +1 disclination on a sphere is screened by a string of dislocations of length $\cos^{-1}(5/6)R \approx 0.59R$ (*22*). We can use the variable linear density of dislocations to compute the total number of excess dislocations $N$ in a scar. We find that $N$ grows for large $(R/a)$ as $(\pi/3)[\sqrt{11} - 5\cos^{-1}(5/6)](R/a)$, $\approx 0.41R/a$, independently of the microscopic potential. This prediction is universal and is in marked agreement with the experiment, as shown by the solid line in Fig. 2.

We expect these scars to be widespread in nature. They should occur, and hence may be exploited, in sufficiently large viral protein capsids, giant spherical fullerenes, spherical bacterial surface layers (s-layers), and the siliceous skeletons of spherical radiolaria (aulosphaera) (*28*), provided that the spherical geometry is not too distorted. Terminating strings of heptagons and pentagons might serve as sites for chemical reactions or even as initiation points for bacterial cell division (*12*) and will surely influence the mechanical properties of spherical crystalline shells.

### References and Notes


1. For the case of a Coulomb potential, see L. Bonsall, A. A. Maradudin, *Phys. Rev. B* **15**, 1959 (1977).
2. H. W. Kroto *et al*., *Nature* **318**, 162 (1985).
3. M. F. Jarrold, *Nature* **407**, 26 (2000).
4. L. Euler, *Opera Omnia*, series i, vol. 26 (Orell Füssli Verlag, 1953); see also www.ics.uci.edu/~eppstein/junkyard/euler.
5. P. Hilton, J. Pedersen, *Am. Math. Month.* **103**, 121 (1996).
6. A value of 12 here is obtained from $6\chi$, where the Euler characteristic $\chi$ of a space is a topological invariant equal to 2 for the sphere.
7. J. J. Thomson, *Philos. Mag.* **7**, 237 (1904).
8. P. Leiderer, *Z. Phys. B* **98**, 303 (1995).
9. D. L. D. Caspar, A. Klug, *Cold Spring Harbor Symp. Quant. Biol.* **27,** 1 (1962).
10. C. J. Marzec, L. A. Day, *Biophys. J.* **65**, 2559 (1993).
11. V. J. Reddy *et al*., *J. Virol.* **75**, 11943 (2001); see also http://mmtsb.scripps.edu/viper/viper.html.
12. U. B. Sleytr, M. Sára, D. Pum, B. Schuster, *Prog. Surf. Sci.* **68**, 231 (2001).
13. D. Pum, P. Messner, U. B. Sleytr, *J. Bacteriol.* **173**, 6865 (1991).
14. N. J. A. Sloane, *Sci. Am.* **250**, 116 (January1984).
15. J. H. Conway, N. J. A. Sloane, *Sphere Packings, Lattices, and Groups* (Springer-Verlag, New York, ed. 3, 1998).
16. The determination of the asymptotics of the ground-state energy of spherical crystals with a logarithmic potential appeared as Problem 7 of Smale's list of key mathematical problems for the 21st century (29).
17. E. L. Altschuler *et. al*., *Phys. Rev. Lett.* **78**, 2681 (1997).
18. T. Erber, G. M. Hockney, in *Advances in Chemical Physics*, I. Prigogine, S. A. Rice, Eds. ( Wiley, New York, 1997), vol. 98, pp. 495–594.
19. D. R. Nelson, *Defects and Geometry in Condensed Matter Physics* (Cambridge Univ. Press, Cambridge, 2002).
20. A. D. Dinsmore *et. al*., *Science* **298**, 1006 (2002). The particular system we explored is obtained by confining cross-linked polystyrene beads (Interfacial Dynamics Corporation, Portland, OR) to the surface of water droplets.
21. B. Delaunay, *Bull. Acad. Sci. USSR Class. Sci. Math. Nat.* **7**, 793 (1934).
22. M. J. Bowick, D. R. Nelson, A. Travesset, *Phys. Rev. B* **62**, 8738 (2000).
23. P. M. Chaikin, T. C. Lubensky, *Principles of Condensed Matter Physics* (Cambridge Univ. Press, Cambridge, 1995).
24. M. J. W. Dodgson, M. A. Moore, *Phys. Rev. B* **55**, 3816 (1997).
25. A. Perez-Garrido, M. A. Moore, *Phys. Rev. B* **60**, 15628 (1999).
26. A. Toomre, personal communication.
27. M. Bowick, A. Cacciuto, D. R. Nelson, A. Travesset, *Phys. Rev. Lett.* **89**, 185502 (2002).
28. O. R. Anderson, *Radiolaria* (Springer-Verlag, New York, 1983).
29. S. Smale, *Math. Intelligencer* **20(2)**, 7 (1998).


30. This work was supported by the U.S. Department of Energy, the National Science Foundation, the Harvard Materials Research Science and Engineering Center (DMR-0213805), the Fonds der Chemischen Industrie, and the Emmy Noether Programme of the Deutsche Forschungsgemeinschaft.

4 December 2002; accepted 29 January 2003